Graphene-based sample supports for *in situ* high-resolution TEM electrical investigations

2011 J. Phys. D: Appl. Phys. 44 055502

(http://iopscience.iop.org/0022-3727/44/5/055502)

IOP PUBLISHING JOURNAL OF PHYSICS D: APPLIED PHYSICS

J. Phys. D: Appl. Phys. **44** (2011) 055502 (7pp) doi:10.1088/0022-3727/44/5/055502

Graphene-based sample supports for *in situ* high-resolution TEM electrical investigations

B Westenfelder[1], J C Meyer[2], J Biskupek[2], G Algara-Siller[2], L G Lechner[2], J Kusterer[3], U Kaiser[2], C E Krill III[4], E Kohn[3] and F Scholz[1]

[1] Institute of Optoelectronics, University of Ulm, Albert-Einstein-Allee 45, 89081 Ulm, Germany
[2] Central Facility of Electron Microscopy, University of Ulm, Albert-Einstein-Allee 11, 89081 Ulm, Germany
[3] Institute of Electron Devices and Circuits, University of Ulm, Albert-Einstein-Allee 45, 89081 Ulm, Germany
[4] Institute of Micro and Nanomaterials, University of Ulm, Albert-Einstein-Allee 47, 89081 Ulm, Germany

E-mail: benedikt.westenfelder@uni-ulm.de

Received 9 September 2010, in final form 22 November 2010
Published 17 January 2011
Online at stacks.iop.org/JPhysD/44/055502

Abstract
Specially designed transmission electron microscopy (TEM) sample carriers have been developed to enable atomically resolved studies of the heat-induced evolution of adsorbates on graphene and their influence on electrical conductivity. Here, we present a strategy for graphene-based carrier realization, evaluating its design with respect to fabrication effort and applications potential. We demonstrate that electrical current can lead to very high temperatures in suspended graphene membranes, and we determine that current-induced cleaning of graphene results from Joule heating.

(Some figures in this article are in colour only in the electronic version)

1. Introduction

Owing to a variety of extraordinary transport properties, graphene has sparked considerable interest in many fields of basic and applied research in recent years [1]. Graphene's structure as an ultrathin layer of carbon atoms imparts unique potential for supporting atomic or molecular samples to permit their visualization via high-resolution transmission electron microscopy (HRTEM) [2–8]. Sample carriers constructed of graphene would be useful not only in static imaging with atomic resolution, but also in the atomic-level visualization of dynamic phenomena, such as thermally activated desorption, drift and diffusion processes. Moreover, the electrical conductivity of graphene makes it conceivable to pass a current through the sample support while simultaneously imaging the sample in the electron microscope. This combination of capabilities would enable, for example, the *in situ* control of local heat generation and the measurement of surface-sensitive electrical conductivities, such as those modified by adsorbate–graphene interactions [9].

The primary difficulty in utilizing graphene in the context of such *in situ* HRTEM investigations is making a reliable electrical connection between an appropriate TEM specimen holder (equipped with a current feedthrough) and a free-standing sheet of graphene. With respect to this technological challenge, only a few successful experiments have been reported in the literature, all of which are based on a particular TEM–scanning tunnelling microscopy (STM) specimen holder made by Nanofactory Instruments AB [10–13]. To obtain a two-point current sourcing system, one electrical contact to the graphene flake is realized by a piezo driven STM tip on the front side, while the other contact is provided by the metallic TEM grid on which the flake is positioned (figure 1(*a*)). As a result, the electrical

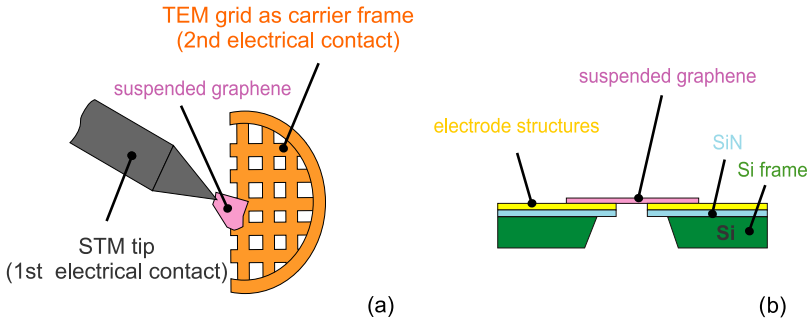

Figure 1. Approaches for *in situ* HRTEM electrical investigations using sample supports incorporating graphene: (*a*) based on a TEM–STM specimen holder [10–12]; (*b*) based on a specially designed sample carrier.

bias between the grid and the STM tip is not well defined spatially, resulting in extremely inhomogeneous distributions of electrical field strength, current density and temperature along the graphene sheet. Moreover, these distributions are systematically nonreproducible, because the absolute current and bias values strongly depend on the detailed electrode geometry.

If measuring the electrical conductivity is not necessary, then *in situ* heating experiments can be carried out in a TEM using commercially available equipment (e.g. Gatan heating holders 628 and 652). In this case, the sample is mounted within a furnace that can be heated by external wiring. However, thermal drift and thermal expansion prevent atomic resolution because a large area surrounding the TEM sample is also heated. At temperatures above 500 °C, water cooling of the heating furnace is required, which introduces additional disturbances arising from the water flow and the additional tubing. In this paper, we present a relatively simple strategy for constructing sample carriers that overcome these deficiencies. The preparation of locally well-defined electrical contacts to the graphene sheet requires this carrier to have an insulating top side, which is realized by a silicon nitride (SiN)-coated silicon (Si) frame. Obtaining the best contrast in TEM when studying deposits on top of graphene and reaching the maximum electrical mobility in the graphene flake both necessitate that the graphene be freely suspended [14]. This is achieved by removing the Si locally below the SiN film and perforating the resulting SiN membrane directly beneath the graphene flake. Electrical contacts are then deposited and structured on the SiN membrane by conventional metal evaporation and optical lithography. Finally, the graphene flake is positioned on these contacts directly above the perforated SiN membrane (figure 1(*b*)). In the following, we describe approaches based on this design to illustrate its considerable advantages over previous graphene-based sample supports.

2. Sample carrier fabrication

2.1. Silicon nitride membrane and silicon frame

The design of conventional TEM systems places certain constraints on the layout of specimen positioning holders, such as the Fischione 2510 biasing holder employed in this study, and on the size of the sample carrier that is attached to the end of the positioning holder. In general, the specimen

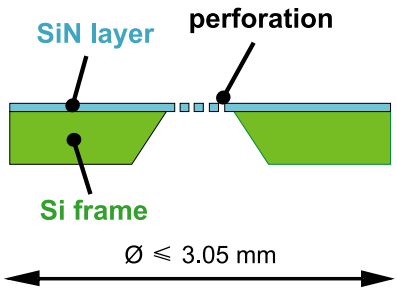

Figure 2. Schematic cross-sectional view of a typical carrier frame for TEM samples.

carrier is limited to a cylindrical region of maximum diameter 3.05 mm and height on the order of 1 mm. Several suppliers offer a variety of Si frames meeting these specifications, some of which can be purchased prefabricated with a top-side membrane of SiN, either with or without perforations (figure 2).

The lateral membrane dimensions, the SiN thickness and both the diameter and the pitch of the holes can typically be selected according to individual requirements (figure 3(*a*)). In order to achieve optimal conditions for the subsequent processing of frames by optical lithography, large, unstructured areas are required. For this reason, commercial suppliers also offer single wafers consisting of individual Si frames joined to each other in the form of so-called multiframe arrays (figure 3(*b*)).

Finally, perforation of the SiN membrane is achieved either again by optical lithography-based dry etching or by cutting via focused ion beam (FIB) etching (figure 4).

2.2. Electrode structures

Fabrication of electrode structures on silicon nitride membranes is usually carried out by optical lithography in conjunction with lift-off of a deposited metal film. However, in the case of the commercial frame variants it is important to consider several complicating factors. As already mentioned, multiframe arrays should be preferred, as they help to avoid the formation of side walls during the photoresist coating process. Otherwise, edge beads formed near the free-standing SiN membrane will not only cause a loss in lithographic resolution but also dramatically reduce the surface area available to lithographic processing (figure 5(*a*)). Furthermore, above a

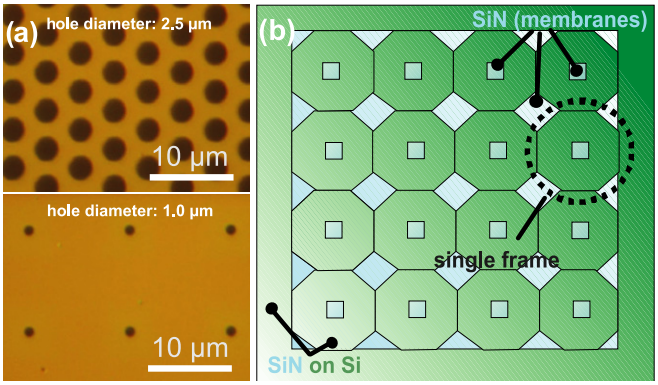

Figure 3. (*a*) Optical micrographs of SiN membranes having two different hole maskings—purchased from Pelco International (top) and Protochips Inc. (bottom). (*b*) Schematic illustration of a multiframe array, purchased from Silson Ltd. Such an arrangement allows the simultaneous processing of several individual carrier frames.

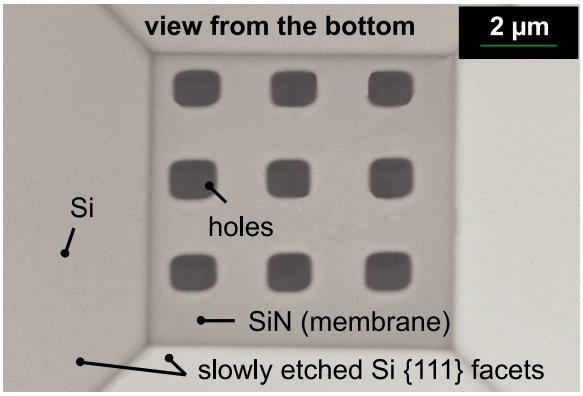

Figure 4. Scanning electron micrograph of the bottom side of a FIB-perforated SiN membrane and the adjacent (1 1 1) Si facets that were created by etching.

certain hole diameter or below a certain hole pitch, resist ripples can arise in the nearby membrane areas, again leading to losses in lithographic resolution (figure 5(*b*)). These ripples originate from the viscosity and surface tension of the photoresist. Moreover, we found that oxygen plasma treatment of the frame surface prior to each resist coating step avoids a repellency of the resist during spin-coating, presumably owing to a change in the SiN/resist interfacial tension. Following processing, the individual frames can be cleaved apart, yielding sample carriers that are ready for graphene positioning (figure 3(*c*)).

2.3. Graphene sheet positioning

Precise positioning of graphene sheets was achieved in this work following the transfer protocol described in [15]. First, the graphene sheet is pressed against a thin, perforated plastic film (thickness of a few nanometres) that is carried by a metal TEM grid. Then, the TEM grid is aligned with the electrode structure by the help of a specially designed translation apparatus and an optical microscope. Finally, the graphene sheet is attached to the electrodes by evaporation of an introduced drop of isopropanol seeping through the interface between the graphene and the electrode surface. The

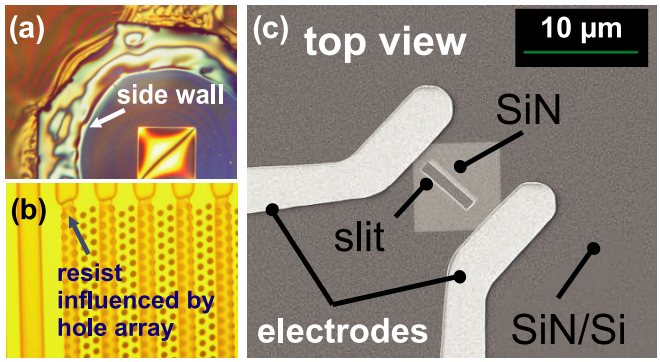

Figure 5. (*a*) Optical micrograph of a resist-coated single frame exhibiting distinct side wall formations at its edges. The side length of the membrane is 0.5 mm. (*b*) Resist ripples on a SiN membrane, in which the resist thickness is locally reduced due to the dense arrangement of 2.5 μm holes. (*c*) Scanning electron micrograph of the top side of a sample carrier with a simple localized electrode geometry and a FIB-perforated free-standing SiN membrane.

plastic and the TEM grid are removed by rinsing in an organic solvent. Typically, some residues remain on the graphene following this procedure, but they can be desorbed by passing an electric current through the graphene [16].

3. Sample carrier design

3.1. Type I: simple localized electrode geometry

The electrode design represents two electrode fingers contacting the graphene (figure 6(*a*)). The membrane holes between the electrodes can be designed to meet a given application's requirements. For example, a smaller number of holes and/or a smaller membrane area can be chosen to improve its mechanical stability. For this purpose it may be advantageous to employ commercially available silicon frames without SiN membrane perforation. It should be noted, however, that in this carrier design the graphene still makes contact with the underlying SiN membrane. On the one hand, owing to the very low heat conductivity of SiN films [17], heat generated in the graphene sheet is not dissipated quickly, which can easily result in temperatures being reached that are higher than the SiN decomposition temperature (figures 6(*b*) and (*c*)). On the other hand, graphene/SiN contact leads to an overall reduction in the electrical mobility of the graphene [14], which significantly lowers the surface sensitivity of conductivity measurements.

3.2. Type II: advanced localized electrode geometry

To eliminate any graphene/SiN support interaction and thereby improve the electrical conductivity of the graphene and achieve a thermally more resistant carrier platform, we developed a new carrier design. Using the metal electrodes as etching masks during a reactive-ion etching (RIE) procedure, we cut a vertical slit through the SiN membrane directly between the electrode pads (figure 7, left). Hence, a sheet of graphene placed on top is suspended only by the two electrodes, making no contact with SiN (figure 7, right).

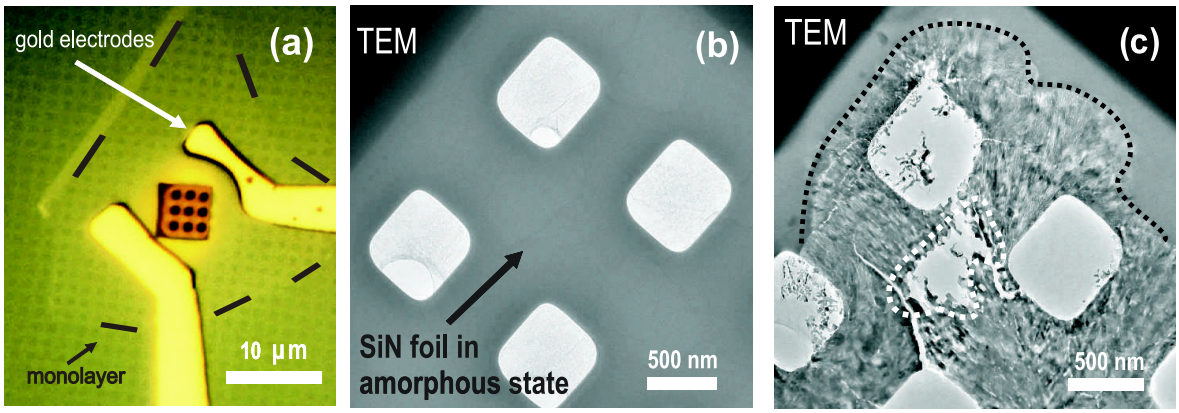

Figure 6. (*a*) Optical micrograph of a sample carrier manifesting a simple localized electrode geometry. Also visible: a graphene monolayer positioned on top of the FIB-perforated SiN membrane (outlined by the black dashed line). TEM images of the same sample at different temperatures: (*b*) state of the graphene-covered SiN membrane at a low sheet current density; (*c*) state of the same membrane at a high sheet current densities ((1–3) $\times$ 10^8 A cm^{-2}) at which crystallization and sublimation of the SiN starts. The black dotted line marks the spatial transition of the SiN membrane from an amorphous into a polycrystalline state, indicating a temperature of approximately 1600 K [18]. The white dotted line marks a region in which the SiN membrane has evaporated, indicating a local temperature in excess of 2000 K.

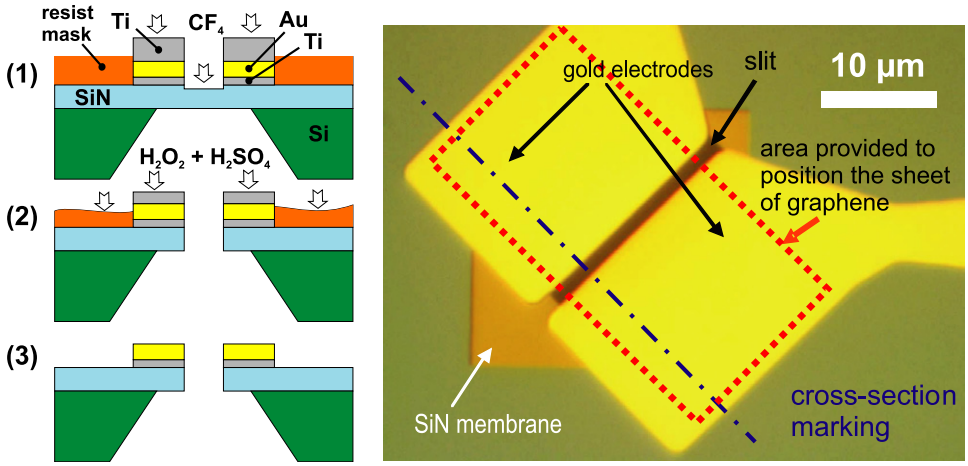

Figure 7. Left: cross-sectional schematic illustration of the layers and the dry- and wet-etching steps performed to achieve the electrode support structure shown on the right. Right: optical micrograph of the advanced sample carrier design on which a graphene sheet is suspended only by gold electrodes.

4. Experiments

To demonstrate the capabilities of our approach, we have performed *in situ* heating investigations of graphene sheets attached to a Type II sample carrier and imaged by an aberration-corrected (CEOS type corrector) FEI 80-300 Titan transmission electron microscope. The microscope was operated at an accelerating voltage of 80 kV in order to stay below the threshold for knock-on damage of graphene [19]. Sample carriers were mounted in a Fischione 2510 biasing TEM holder, and an electrical current was passed through the graphene sample by applying an appropriate voltage between the electrodes. Gold nanoislands deposited on the graphene (figure 8) acted as indicators for the heat generated by the applied current [20, 21].

At a current of about 4 mA—which corresponds to a current density of about 2 $\times$ 10^7 A cm^{-2} in the graphene sheet—a remarkable change in shape of the gold nanoislands was observed. The initially flat particle shape becomes more spherical, suggesting that the corresponding increase in temperature allowed the nanoislands to minimize their surface area-to-volume ratio. The distribution of particle shapes is therefore a measure for the spatial temperature profile across the graphene sheet (figure 9). In the vicinity of the electrodes, the locally produced heat is drained more efficiently, leading to comparably lower temperatures than in the central region of the suspended graphene sheet. This interpretation is in agreement with the observation that gold nanoislands first begin to disappear in the centre of the graphene membrane.

Gold particles that were exposed to the electron beam prior to current-induced annealing are surrounded by visible layers and shells of amorphous carbon. We assume that the latter originate from mobile hydrocarbons produced by electron-beam cracking of contamination species. Apparently, the amorphous carbon shells keep the gold particles in place even in the liquid state. Moreover, we found that the amorphous carbon layers could not be removed by further Joule heating of the graphene sheet. Gold particles located in regions that

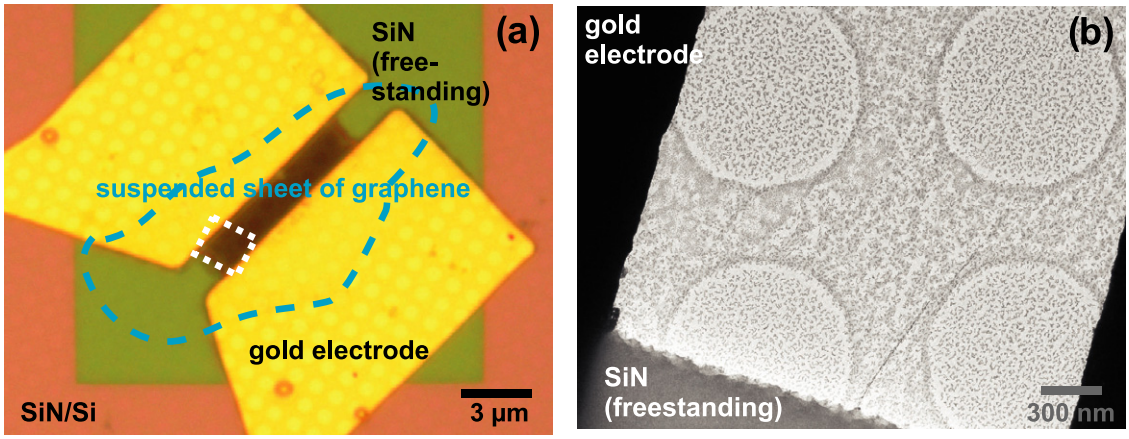

Figure 8. Images of a graphene sheet suspended between gold electrodes. (*a*) Optical micrograph: the blue dashed curve outlines the graphene, and the white dashed box indicates the area shown on the right. (*b*) TEM image taken at low sheet current density: the sheet is covered with gold nanoislands (tiny grey spots) and plastic residue visible at the edges of the circles. The latter originate from the perforated plastic foil used in the graphene positioning process.

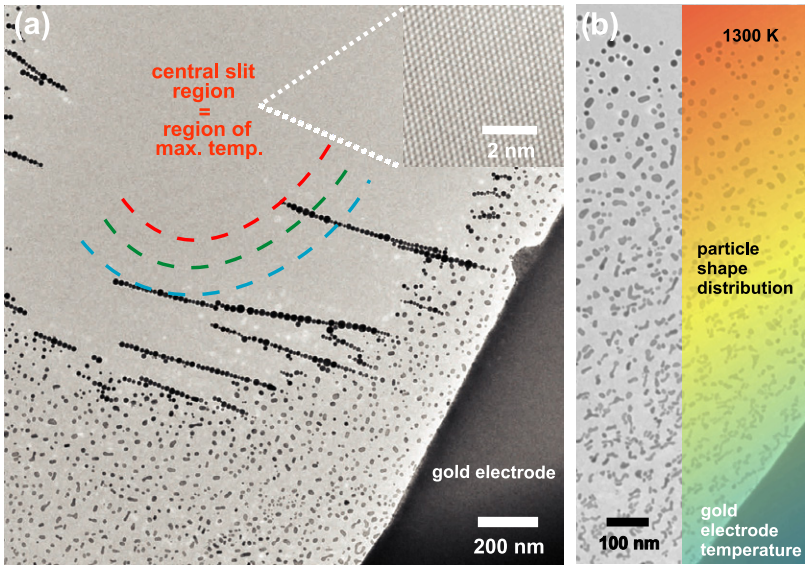

Figure 9. TEM image of graphene subjected to a high sheet current density. (*a*) Contamination is removed from regions of high temperature. We observed that gold nanoislands deposited on the graphene surface were partly arranged in straight lines. Schematically drawn isotherms illustrate a temperature profile roughly hinted at by the distribution of particle shapes. (*b*) Different nanoisland shapes correspond to the presence of a temperature gradient across the graphene sheet.

were not exposed to the electron beam prior to Joule heating, however, disappear without any residue and leave behind atomically clean graphene areas (figure 9). Hence, in order to obtain clean graphene membranes in the TEM, current-induced Joule heating must be applied prior to electron-beam exposure.

Figure 10 shows gold nanocrystals contained within amorphous carbon shells at different temperatures. The applied current density of the graphene sheet is approximately $10^7\,\mathrm{A\,cm^{-2}}$. The smallest particle visible in figure 10(*a*), which has a diameter of 5 nm, is already molten. In figure 10(*b*), the same region is shown after a slight increase in current density. At this correspondingly higher temperature, the larger particles have begun to melt. At a still higher current density, the drops start to evaporate (figure 10(*c*)), with complete disappearance of both particles taking place within approximately 2 min.

5. Discussion

In a recently published investigation of heat-induced transformations of gold nanocrystals in a TEM, the particles were supported by silicon nitride and amorphous carbon [22]. In contrast, our approach is based on graphene as a support material, which results in much higher contrast, enabling real-time visualization of heat-induced phenomena with atomic resolution.

Other Joule heating experiments are based on graphene as a support material [13], but—as already mentioned above—result in a highly inhomogeneous spatial distribution of the electrical current density. Moreover, the reproducibility of such STM tip based approaches is limited by a random electrode alignment. Therefore, the local amount of the electrical power density in the graphene support is not well

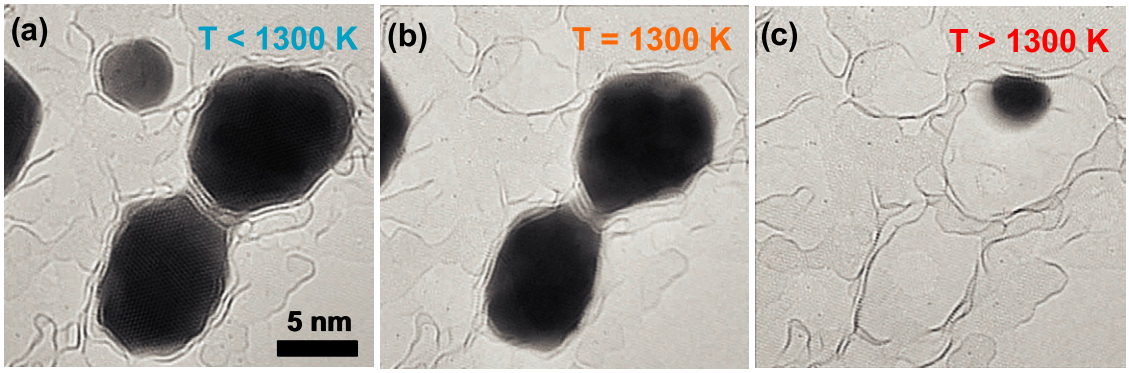

Figure 10. HRTEM images of gold nanoislands changing their state of aggregation as a function of temperature: (*a*) below 1300 K, the crystalline structure of the two larger gold particles is still visible; (*b*) at 1300 K, the atomic planes have disappeared, implying that the particles have transformed to the liquid state; (*c*) above 1300 K, evaporation sets in.

known making the investigation of heat sensitive deposits difficult.

Our approach uses a custom-designed electrode geometry enabling a precise adjustment and determination of the locally generated heat, i.e. of the local current density. We obtain a temperature distribution with a maximum temperature at the centre of the membrane and a smooth temperature gradient towards the electrodes, as indicated in figure 9(*a*). This allows one to obtain a complete temperature-variation profile for the adsorbed objects in a single exposure, as demonstrated in figure 9(*b*).

The results described here about gold nanoparticles are just one example for significantly improved TEM imaging in conjunction with *in situ* experimentation. We believe that the great potential of this sample carrier concept will be an important step towards further *in situ* electrical heating and *in situ* electrical sensing experiments on various objects deposited on graphene to study their intrinsic nature and their interaction with such monolayer support materials.

6. Conclusions

We developed a graphene-based sample carrier concept that satisfies the demands for *in situ* investigation of thermal and electrically induced effects at the atomic level in a TEM. A simple carrier design was presented, which is well suited to studying heat-induced phenomena on graphene. We also presented a more advanced design which provides greater surface sensitivity in electrical conductivity measurements and a higher heat resistance. In our experiments performed with the advanced sample carrier we observed the cleaning of graphene by Joule heating, resulting in atomically clean membranes in the hottest areas and shape changes of gold nanoparticles in the moderately hot regions. Furthermore, the study of atomically resolved Au nanoislands deposited on graphene sheets demonstrated that our graphene-based sample carrier is useful not only as a quasi-transparent substrate for high-resolution TEM but also as a platform for *in situ* investigations of the effects of electrical current on atomic and molecular species and their heat-induced dynamics.

Acknowledgments

We thank Ilona Argut for technical assistance. Furthermore, this work was supported by the DFG (German Research Foundation) and the Ministry of Science, Research and the Arts (MWK) of Baden-Württemberg in the frame of the SALVE (Sub-Angstrom Low-Voltage Electron microscopy) project.

References

[1] Geim A K and Novoselov K S 2007 *Nature* **6** 183–91
[2] Dobelle W H and Beer M 1968 *J. Cell Biol.* **39** 733–5
[3] Booth T J, Blake P, Nair R R, Jiang D, Hill W E, Bangert U, Bleloch A, Gass M, Novoselov K S, Katsnelson M I and Geim A K 2008 *Nano Lett.* **8** 2442–46
[4] Meyer J C, Girit C O, Crommie M F and Zettl A 2008 *Nature* **454** 319–22
[5] Meyer J C, Kisielowski C, Erni R, Rossel M D, Crommie M F and Zettl A 2008 *Nano Lett.* **8** 3582–6
[6] Kaiser U, Chuvilin A, Meyer J C and Biskupek J 2009 *Materials Science Microscopy Conf. MC2009 (Graz, Austria)* ed W Grogger *et al* vol 3 pp 1–6
[7] Lee Z, Jeon K-J, Dato A, Erni R, Richardson T J, Frenklach M and Radmilovic V 2009 *Nano Lett.* **9** 3365–69
[8] Pantelic R S, Meyer J C, Kaiser U, Baumeister W and Plitzko J M 2009 *J. Struct. Biol.* **170** 152–6
[9] Schedin F, Geim A K, Morozov S V, Hill E W, Blake P, Katsnelson M I and Novoselov K S 2007 *Nature Mater.* **6** 652–5
[10] Jia X, Hofmann M, Meunier V, Sumpter B G, Campos-Delgado J, Manuel Romo-Herrera J, Son H, Hsieh Y, Reina A, Kong J, Terrones M and Dresselhaus M S 2009 *Science* **323** 1701–5
[11] Hiang J Y, Ding F, Yakobson B I, Lu P, Qi L and Li J 2009 *Proc. Natl Acad. Sci.* **106** 10103–8
[12] Qi L, Huang J Y, Feng J and Li J 2010 *Carbon* **48** 2354–60
[13] Kim K, Regan W, Geng B, Alemán B, Kessler B M, Wang F, Crommie M F and Zettl A 2010 *Phys. Status Solidi RRL* **4** 302–4
[14] Chen J, Jang C, Xiao S, Ishigami M and Fuhrer M S 2010 *Nature Nanotechnol.* **3** 206–9
[15] Meyer J C, Girit C O, Crommie M F and Zettl A 2008 *Appl. Phys. Lett.* **92** 123110
[16] Moser J, Barreiro A and Bachtold A 2007 *Appl. Phys. Lett.* **91** 163513

[17] Griffin A J, Brotzen F R and Loos P J 1994 *J. Appl. Phys.* **76** 4007–11
[18] Li Y, Liang Y, Zheng F, Shong X and Hu Z 1994 *J. Mater. Sci. Lett.* **13** 1588–90
[19] Zobelli A, Gloter A, Ewels C P, Seifert G and Colliex C 2007 *Phys. Rev.* B **75** 245402
[20] Begtrup G E, Ray K G, Kessler B M, Yuzvinsky T D, Garcia H and Zettl A K 2007 *Phys. Rev. Lett.* **99** 155901
[21] Buffat Ph and Borel J-P 1976 *Phys. Rev.* A **13** 2287–98
[22] Young N P, van Huis M A, Zandbergen H W, Xu H and Kirkland A I 2010 *Ultramicroscopy* **110** 506–16